ELSEVIER

Materials Science and Engineering A xxx (2007) xxx–xxx

MATERIALS SCIENCE & ENGINEERING A

www.elsevier.com/locate/msea

Shape memory effect and superelastic behavior of TiNi shape memory alloy processed by vacuum plasma spray method

Hiroyuki Nakayama [a], Minoru Taya [a,*], Ronald W. Smith [b], Travis Nelson [b], Michael Yu [c], Edwin Rosenzweig [c]

[a] *Center for Intelligent Materials and Systems, Department of Mechanical Engineering, University of Washington, Box 352600, Seattle, WA 98195-2600, United States*

[b] *Materials Resources International, 811 W. Fifth Street/Unit 2, Lansdale, PA 19446, United States*

[c] *Naval Air Systems Command, 48066 Shaw Road, Unit 5, Bldg 2188, Patuxent River, MD 20670, United States*

Received 12 August 2006; received in revised form 14 December 2006; accepted 18 January 2007

Abstract

Machining of TiNi shape memory alloy into a complicated three-dimensional (3D) shape is quite difficult, thus a near-net shape forming of 3D shaped TiNi alloy is attractive and cost-effective. Vacuum plasma spray (VPS) process is one of such near-net shape forming processes. In this paper, two kinds of thick TiNi layer, Ni-rich and Ti-rich compositions, were fabricated by VPS process and their shape memory effect (SME) and superelastic (SE) behaviors were characterized. As-VPS processed Ni-rich TiNi which was subjected to homogenization at 1163 K for 7.2 ks and subsequent aging at 773 K for 18 ks exhibited good martensitic transformation behavior. The recoverable strain of the TiNi alloys due to SME and SE behavior were measured to be 2.4% and 5.0%, respectively. The Ti-rich TiNi alloy also exhibited good martensitic transformation behavior and SME in the as-homogenized state.

Keywords: Vacuum plasma spray (VPS); Near-net shape; Stress–strain curve; Superelastic behavior; Shape memory effect; Martensitic transformation; TiNi alloy

1. Introduction

TiNi shape memory alloys are widely used in many applications such actuators, due to their excellent shape memory effect (SME) and superelastic (SE) behaviors. However, the TiNi alloys have poor cold workability due to their high work-hardening rate [1]. An elongation of Ti–50.0 at.% Ni alloy is about 18% at room temperature. When Ni content exceeds 51.0 at.%, the cold working of such TiNi alloy becomes very difficult [2]. Therefore, hot working at around 1073 K is normally applied to TiNi alloys, which inevitably gives rise to thick oxide layer on the TiNi surface, degrading their SME and SE properties. Due to the difficulty of the machining of TiNi alloys, we must use a tungsten carbide tool whose use life is short, thus, often we end up with using electron discharge machining which is more costly. One of the solutions to overcome these problems is use of near-net shape process by powder metallurgy (PM).

Several researchers reported SME and SE behaviors of as-PM processed TiNi alloys [3–7]. Kato et al. reported about 6% SE and 7% SME strains in TiNi alloy that was hot-isotropically pressed [3,4]. It is noted that the material produced by PM tends to eliminate internal voids. In addition, the sintering usually utilizes solid–solid reaction between powders with the results that the particle boundary is weaker than grain boundary, leading to reduction in the mechanical properties of as-sintered materials. Particularly, fracture strain and fatigue properties of PM-processed materials are reduced [4,5].

Vacuum plasma spray (VPS) process is one of the spraying methods. Source powders are injected to plasma stream where the injected material is melted immediately by a high temperature plasma jet, and then the molten metal particles are accelerated in the plasma jet stream to deposit as overlapping "splats" onto a substrate to form a P/M consolidated deposit. The source powders are melted by the plasma jets and the sprayed layers become high density. However, during VPS process oxide and nitrides more likely to form, due to the extremely high temperature plasma jet. In particular, titanium in a TiNi alloy has a strong affinity with oxygen, so that titanium oxides or nitrides

* Corresponding author. Tel.: +1 206 685 2850; fax: +1 206 685 8047.
E-mail address: tayam@u.washington.edu (M. Taya).

0921-5093/$ – see front matter © 2007 Published by Elsevier B.V.
doi:10.1016/j.msea.2007.01.053

Table 1
Results of composition analysis of source powders and sprayed TiNi alloy

	NiTi sample (Ni-rich)		TiNi sample (Ti-rich)	
	Original TiNi powder (wt.%)	Sprayed TiNi (wt.%)	Original TiNi powder (wt.%)	Sprayed TiNi (wt.%)
Ni	56.8 (51.9 at.%)	55.6 (51.3 at.%)	54.7 (49.7 at.%)	54.4 (49.5 at.%)
Ti	43.0 (48.1 at.%)	42.9 (48.7 at.%)	45.2 (50.3 at.%)	45.2 (50.5 at.%)
O	0.120	0.230	0.066	0.101
N	0.002	0.006	0.003	0.025
C	0.065	0.11	0.011	0.008
Others	Balance	Balance	Balance	Balance

can be formed easily during the process. Thus, control of atmosphere, preferably in high vacuum is desired. Characterization of as-VPS processed TiNi alloys has been reported by several researchers [8–11]. However, the previous studies were focused on very thin film TiNi (under 100 μm), where the formation of oxide, nitride and other intermetallic compounds were observed. There have been no studies on SME and SE behavior of sprayed TiNi alloys of relatively large size.

In this paper, the experimental results of VPS processing of TiNi alloys under low oxygen atmosphere will be reported and their heat treatment effects on SME and SE behaviors assessed by compression testing will be examined. The microstructures of as-VPS processed, heat-treated TiNi alloys are characterized by XRD and TEM with aim of elucidating the merits of VPS processing of TiNi alloys and the mechanisms responsible for their improved SME and SE properties.

2. Experimental procedure

Two kinds of TiNi alloy powders, Ni-rich composition and Ti-rich composition, were sprayed on a steel pipe substrate of outer diameter being 31.8 mm with 1.7 mm wall thickness. The sprayed TiNi layers were more than 15 mm thick. The composition of powders and sprayed materials are listed in Table 1. Hereafter, the Ni-rich sample and Ti-rich sample are called as 'NiTi' and 'TiNi', respectively. The composition of the sprayed materials is found to be the same as those of the starting powders. Contaminations by oxygen, nitrogen and carbon were also observed in the powders and sprayed materials. However, the level of contaminations of NiTi and TiNi remained the same as the source powders. For characterization of sprayed materials, the surface layer of as-VPS processed material was taken out from substrate and machined to cylindrical bar of diameter 5 mm. The machined cylinders were subjected to homogenized heat treatment at 1163 K for 7.2 ks under vacuum atmosphere. Subsequent aging treatments were also carried out to some of the homogenized materials in air or vacuum, followed by water or helium quenching. Transformation temperatures of the as-VPS processed material with and without heat treatment were measured by differential scanning calorimetry (Perkin-Elmer, DSC 6) with heating and cooling rate of 20 K/min and 10 K/min, respectively. The measured transformation temperatures were martensitic transformation start (M_s) and finish (M_f), austenitic transformation start (A_s) and finish (A_f) and R-phase transformation start (R_s) and finish (R_f). After the heat treatment, compression testing, limited thermal cycle testing and stress cycle testing were applied to selected specimens. The specimens for the mechanical testing were machined to cylindrical shape with 5 mm in diameter and 5 mm in height using electrical discharging machine. X-ray diffraction (XRD) was also performed to determine the formed phases in the VPS processed specimens using Cu Kα radiation. Microstructural observations were conducted on selected specimens by transmission electron microscope (TEM) operated at 120 kV. Samples for TEM observations were prepared by electro-chemical polishing using H_2SO_4:methanol = 2:8 (vol.) solution.

3. Experimental results

The XRD results of as-sprayed and as-homogenized NiTi and TiNi are shown in Fig. 1. The as-sprayed NiTi is found to be predominantly composed of austenite phase. In addition, the minor peaks, indicated by open squares in Fig. 1, corresponding to martensite phase are seen in the vicinity of the austenite phase peak. This is attributed to non-uniform distribution of TiNi composition. After the homogenization, the XRD pattern is found to be similar to the as-sprayed state, suggesting that some degree of the unevenness of composition still remains after the homogenization. In the case of TiNi specimen, its majority is composed of martensite phase with austenite phase as minority. Even though the homogenization treatment was applied, the TiNi specimen is still composed of martensite phase and austenite phase. Therefore, the TiNi specimen still has an unevenness of composition after the homogenization. However, in both NiTi and TiNi samples, no unfavorable oxides, nitrides and intermetallic compound phases were observed in theses XRD results. These results indicate that theVPS processed materials are composed by TiNi austenite phase and martensite phase dominantly, and the amounts of other unfavorable phases remain very modest. Therefore, this demonstrates that VPS process provides clean NiTi and TiNi materials.

The DSC curves of as-sprayed and as-homogenized NiTi and TiNi are shown in Fig. 2. In the case of NiTi, no significant transformation peaks were observed in both of the as-sprayed and as-homogenized specimens. This is because the transformation temperatures were lower than the temperature range measured by DSC. The estimated M_s temperature from the composition of NiTi specimen was below 170 K [12]. In contrast, TiNi in the as-sprayed state exhibits the martensitic and reverse martensitic transformation behavior, where

Please cite this article in press as: H. Nakayama et al., Mater. Sci. Eng. A (2007), doi:10.1016/j.msea.2007.01.053

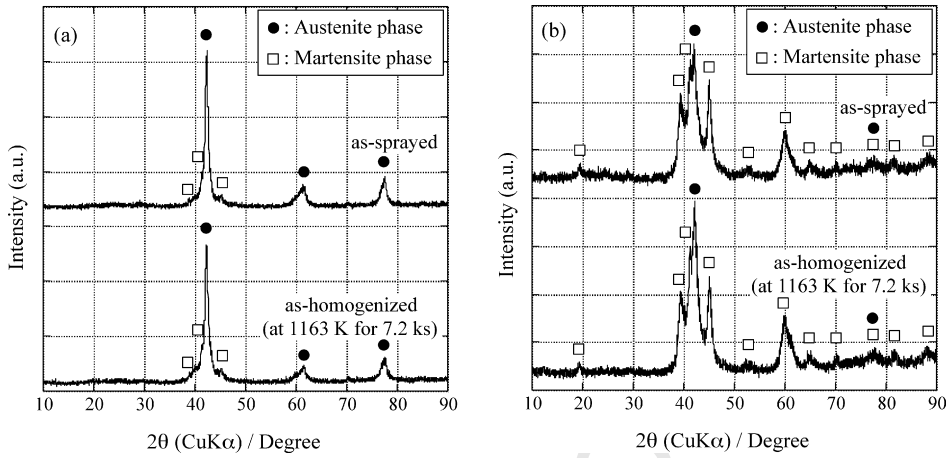

Fig. 1. XRD profiles of as-sprayed and as-homogenized state in (a) NiTi sample and (b) TiNi sample.

the measured transformation temperatures were $M_s = 339$ K, $M_f = 320$ K, $A_s = 351$ K and $A_f = 379$ K. After the homogenization treatment, the transformation peaks become sharper than that of as-sprayed material, and all of transformation temperatures were increased as compared with the as-VPS processed specimen. The transformation temperatures of as-homogenized TiNi specimen were $M_s = 342$ K, $M_f = 330$ K, $A_s = 363$ K and $A_f = 385$ K. The changes in the DSC profiles implied that the unevenness of composition was alleviated by the homogenization. The enthalpy changes in reverse transformation in as-sprayed and as-homogenized TiNi materials are 26.10 and 25.50 J/g, respectively. These values are found to be higher than those of bulk TiNi alloy previously reported [13].

Fig. 3 shows the changes in the transformation temperatures by the aging at 773 K in the NiTi specimen. The as-homogenized sample (Fig. 3(a)) did not show any peaks. The heat treatment at 773 K for 2.4 ks in air (Fig. 3(b)) caused the R-phase transition and martensite phase transition on the cooling, and austenite phase transition on the heating. However, the transformation peaks are broad. By increasing aging time (7.2 ks, Fig. 3(c)), the shapes of all peaks become sharper, and the transformation temperatures are increased. After 18 ks aging (Fig. 3(d)), the shapes of peaks are slightly sharper than those of the specimen with 7.2 ks aging. However, all of transformation temperatures except for M_f are almost the same as those of the 7.2 ks aged sample. The transformation temperatures after aging for 18 ks are $M_s = 262$ K, $M_f = 249$ K, $A_s = 294$ K, $A_f = 311$, $R_s = 320$ K and $R_f = 293$ K. Fig. 3(e) shows the DSC behavior of the samples aged in a vacuum atmosphere at 773 K for 18 ks followed by He quenching. The transformation behavior is similar to the aged sample under air. However, the transformation temperatures of (e) are higher than those of (d). The reason for change in transformation temperature by aging in the NiTi specimen is considered to be due to the crystallization of amorphous phase or precipitation. In this case, we believe that the change in the transformation temperatures were due to precipitation, because the Ti_3Ni_4 precipitates were observed by TEM (see Fig. 4), and no amorphous phase was detected by XRD and TEM. The detailed mechanism

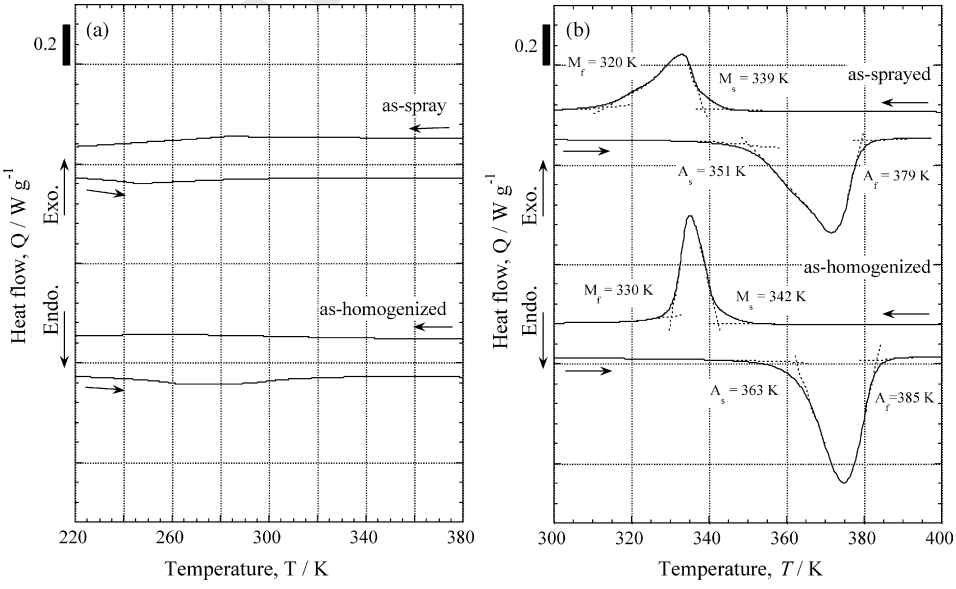

Fig. 2. DSC curves of as-sprayed and as-homogenized state in (a) NiTi sample and (b) TiNi sample.

Please cite this article in press as: H. Nakayama et al., Mater. Sci. Eng. A (2007), doi:10.1016/j.msea.2007.01.053

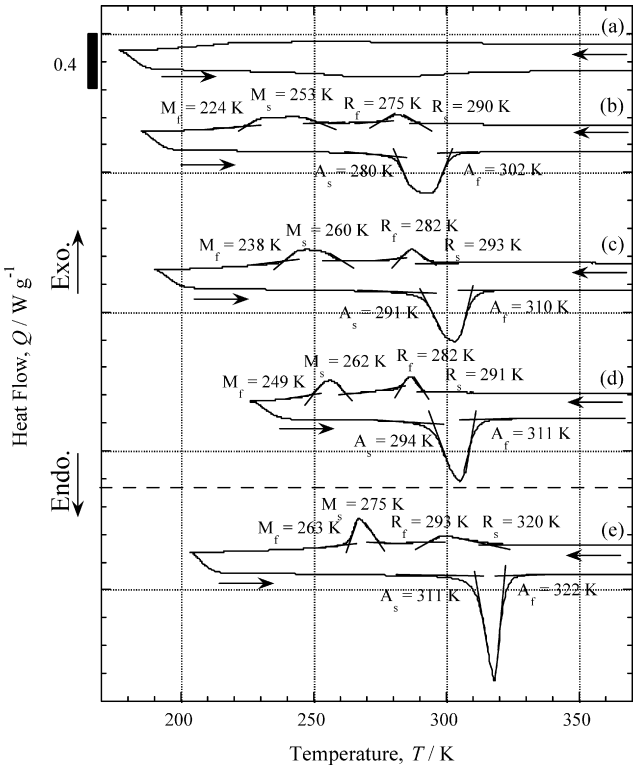

Fig. 3. DSC curves of NiTi sample after (a) homogenization, and subsequent aging at 773 K (b) for 2.4 ks, (c) for 7.2 ks, (d) for18 ks under air and (e) for 18 ks under vacuum condition.

of the change in transformation temperatures by precipitations is described later.

Fig. 4 shows the TEM bright field image of the NiTi sample which was homogenized and aged at 773 K for 18 ks under air, where the selected area diffraction (SAD) pattern obtained from the image is shown to the right. The electron beam is almost parallel to $[1\,1\,0]_{B2}$ direction. The several precipitates with lenticular shape are seen. These precipitates were not observed in the sample of as-homogenized state. By the analysis of the SAD pattern, it is confirmed that the lenticular precipitates exist along $(1\,1\,1)_{B2}$ plane. The metastable Ti_3Ni_4 phase is known to have lenticular shape and they are oriented along the $(1\,1\,1)_{B2}$ due to their coherency with B2 matrix [14]. Therefore, the precipitates observed by this TEM study are identified as Ti_3Ni_4. The formation of Ni-rich precipitation can lead to increasing of Ti content in TiNi matrix. Martensitic and reverse transformation temperatures are sensitive to alloy composition. Reduction of 0.1 at.% Ni leads to an increment of transformation temperature of about 10 K [12]. Therefore, the transformation temperature of the NiTi sample is increased by a change in the composition of TiNi matrix due to aging effect. The enthalpy of transformations of Fig. 3(d) obtained from the area of DSC peaks are −8.49 J/g for martensitic transformation, −4.12 J/g for R-phase transformation and 14.64 J/g for reverse transformation. The values of the enthalpy of the reverse transformation (14.64 J/g) is comparable to that reported on reverse transformation in a bulk TiNi alloy (15.80 J/g) [13], indicating that the sprayed TiNi alloy exhibits SME and SE properties similar to bulk materials. The effects of the aging treatment were also examined for TiNi specimen. No significant change in transformation temperatures was found in the aged TiNi sample. The similar results were reported [15]. This is, probably, due to the difference in the precipitation process between TiNi and NiTi.

The results of compression testing of NiTi aged at 773 K for 18 ks under air are shown in Fig. 5, where (a) is the stress–strain curve tested at M_f temperature (249 K) which exhibits SME behavior. The residual strain after un-loading (2.4%) becomes zero upon temperature increase above A_f temperature, as shown by arrow, indicating perfect SME behavior, Fig. 5(a). The stress–strain curve tested near A_f temperature (304 K) shown in Fig. 5(b) exhibits good SE behavior. The onset stress and strain of the stress-induced martensite are 400 MPa and 2.2%, respectively. The strain of slightly over 5.0% can be recovered after un-loading, which is a large superelastic strain. By increasing

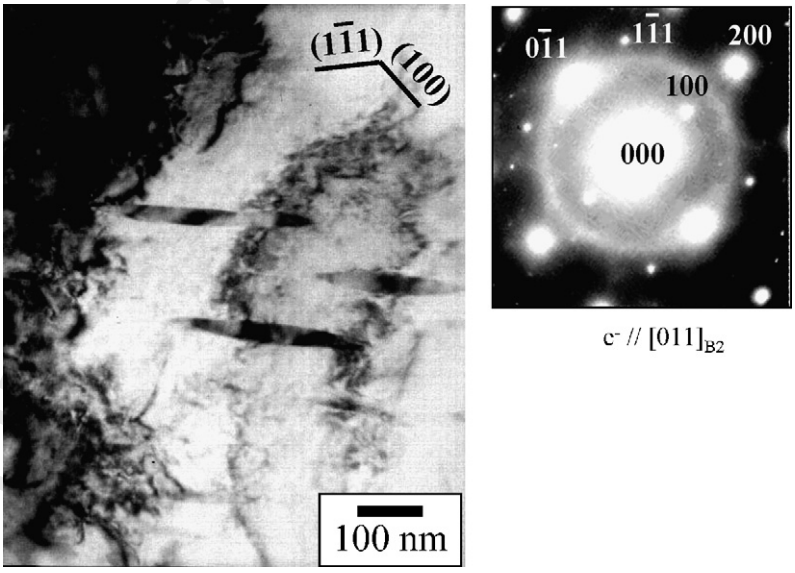

Fig. 4. TEM image of NiTi sample aging at 773 K for 18 ks under air, where incident electron beam is almost parallel to $[0\,1\,1]_{B2}$ direction.

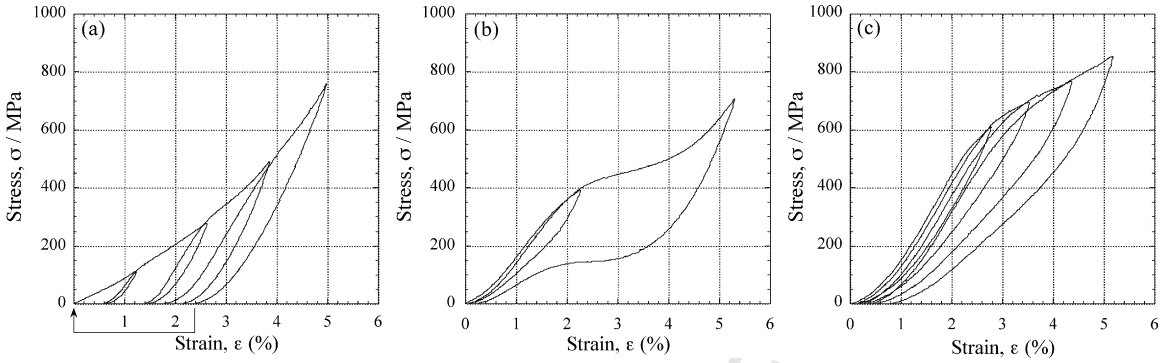

Fig. 5. Stress–strain curves of NiTi sample aged at 773 K for 18 ks under air tested at (a) 249 K, (b) 304 K and (c) 320 K.

testing temperature to above A_f (320 K) (Fig. 5(c)), the superelastic behavior is still observed, but with unrecoverable strain of 0.8%. This is because the increased testing temperature leads to increase the onset stress for the stress-induced martensite, while reducing the yield stress, hence resulting in partial plastic deformation.

The stress–strain curves of TiNi in as-homogenized state are shown in Fig. 6. The TiNi sample tested at room temperature (RT) exhibits SME effect. The recoverable SME strain by heating at 473 K after deformation is about 4.0% as indicated by arrow. This value is comparable to that of a bulk TiNi shape memory alloy. It is noted in Fig. 6(b) that TiNi sample tested at around A_f temperature (384 K) does not show any SE behavior, i.e. only plastic deformation is observed. This is attributed to the fact that the high testing temperature decreases the yield strength of the TiNi austenite phase, which is below the onset stress for stress-induced martensite, resulting in the plastic deformation before the formation of stress-induced martensite phase. Liu et al. reported the plastic yielding of TiNi alloy above 350 K, whose M_s temperature was about 305 K, due to the same mechanism mentioned above [16].

Fig. 7(a) shows the result of thermal cyclic testing of NiTi sample aged at 773 K for 18 ks under vacuum. The pre-stress compression of 250 MPa was applied on NiTi sample at RT and kept during the test. From the stress–strain curve of the sample shown in Fig. 7(b), it is clear that the sample was in stress-induced martensite state under pre-stress as indicated by solid triangle. The strain recovers due to reverse transformation at 330 K on first heating and deformed again by martensitic transformation at 297 K on cooling. These testing temperatures are higher than the A_s and M_s detected by the DSC without pre-stress, see Fig. 3(e). The constant stress can promote the martensitic and reverse martensitic transformation that take place at higher temperatures. The change in transformation temperature under constant stress can be estimated by Clausisu–Clapeyron equation as follows [17]:

$$\frac{d\sigma}{dT} = -\frac{\Delta H}{\varepsilon T}, \quad (1)$$

where ΔH (=−12.45 J/g) is an enthalpy change due to martensitic transformation, ε (≈2.5%) a transformation strain and T (≈$(M_s + A_s)/2$) is an equilibrium temperature. The estimated value of $d\sigma/dT$ based on $\Delta H = -12.45$ J/g is 11.0 MPa/K, which is in good agreement with the experimental value obtained from Fig. 7(a) ($d\sigma/dT = 250$ MPa/22 K = 11.4 MPa/K). The recovered strain by first heating is about 1.2%, Fig. 7(a). However, on the cooling, the strain does not revert to zero, i.e. about 0.13% permanent strain remained in the sample at the end of first cooling cycle. By increasing thermal cycles under constant stress, the permanent strain increases. After 15 cycles, the strain–temperature curve is almost saturated. The recoverable strain after 15 cycles is about 0.6%. Even though the amount

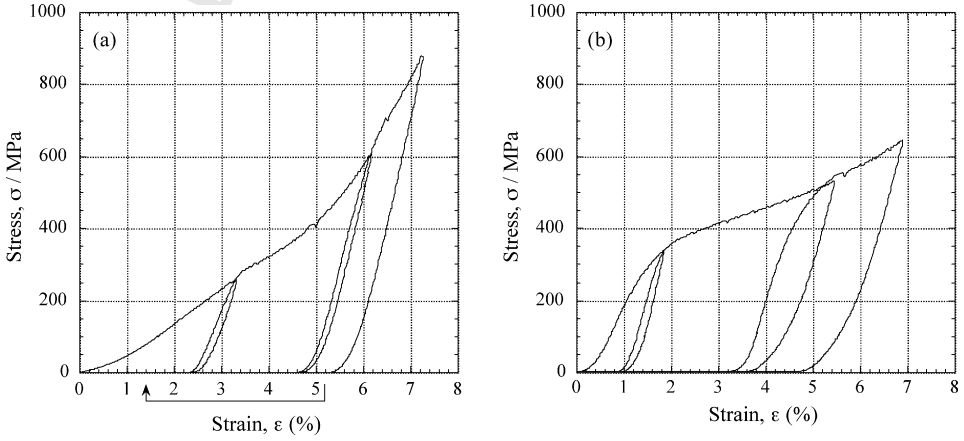

Fig. 6. Stress–strain curves of TiNi sample in as-homogenized state tested at (a) RT and (b) 384 K.

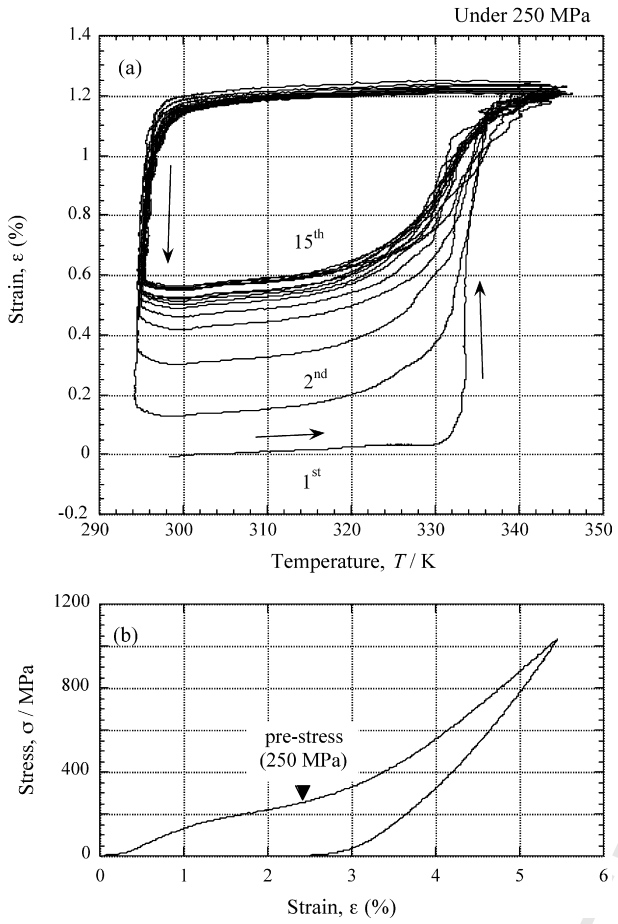

Fig. 7. (a) Results of thermal cyclic testing under constant stress in aged NiTi sample at 773 K for 18 ks under vacuum. (b) Stress–strain curve of the NiTi sample where the state of sample under pre-stress compression is indicated by solid triangle.

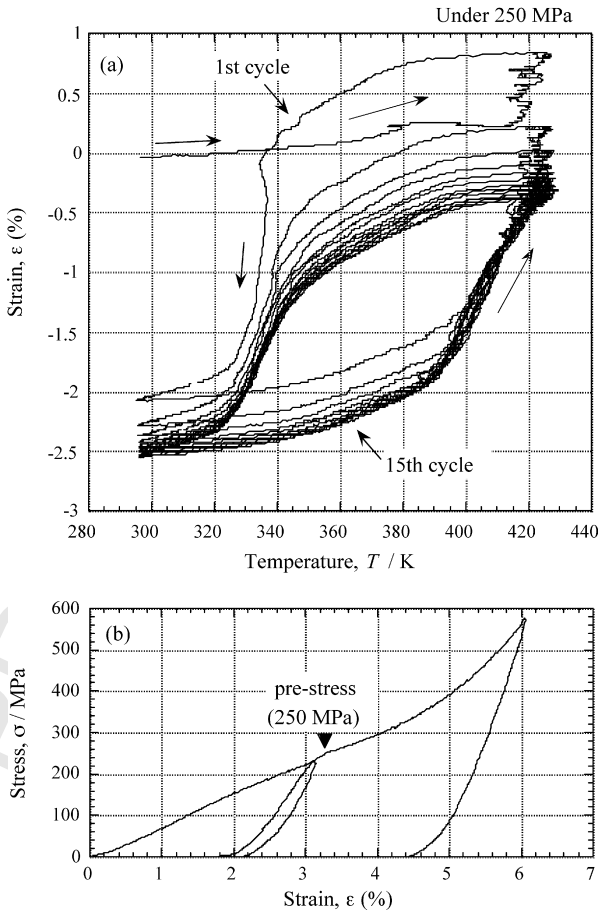

Fig. 8. (a) Results of thermal cyclic testing performed under constant stress in TiNi sample where the samples are homogenized and aged at 773 K for 18 ks under vacuum before testing. (b) Stress–strain curve of the sample tested at RT where the state of sample under pre-stress compression is indicated by solid triangle.

of the recoverable strain is as small as 0.6%, the repeatable strain–temperature cycle behavior after 15 cycles is considered useful for use in some applications.

The results of thermal cyclic testing of TiNi sample aged at 773 K for 18 ks under vacuum condition are shown in Fig. 8. The TiNi sample was pre-deformed by 250 MPa compression stress at RT, where the sample was deformed in martensite state shown in Fig. 8(b). On the first heating, the sample recovers at 413 K. However, the SME strain is small, which is about 0.6%, Fig. 8(a). On the first cooling, the TiNi sample starts to shrink at 333 K due to martensitic transformation. By further cooling, the sample shrinks to shorter length than the initial length. After the second cycle, the temperature–strain curves exhibit hysteresis loop. The permanent strain is accumulated by increasing cycle number, while recoverable strain is decreased with increasing cycle number. The hysteresis loop is almost saturated after 15th cycle. The available strain after 15 cycles is about 2.2%, which is relatively large, thus useful range for several applications. The small SME strain on the first heating is due to the plastic deformation of the sample. The schematic relationship between the reverse transformation temperatures (A_s and A_f) and yield stress (σ_y) is shown in Fig. 9. In the case of TiNi sample having relatively higher transformation temperatures, the stress at A_s temperature and yield stress are nearly the same under the applied constant stress condition, thus the sample can go into plastic deformation (hatched) region by increasing temperature before achieving the stress at A_f. Here, the direction of SME

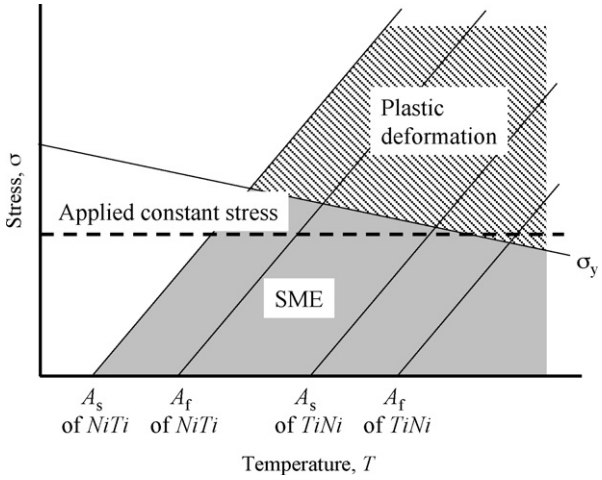

Fig. 9. Schematic relationship between reverse transformation temperatures (A_s, A_f) and yield stress (σ_y) of shape memory alloy in stress–temperature diagram.

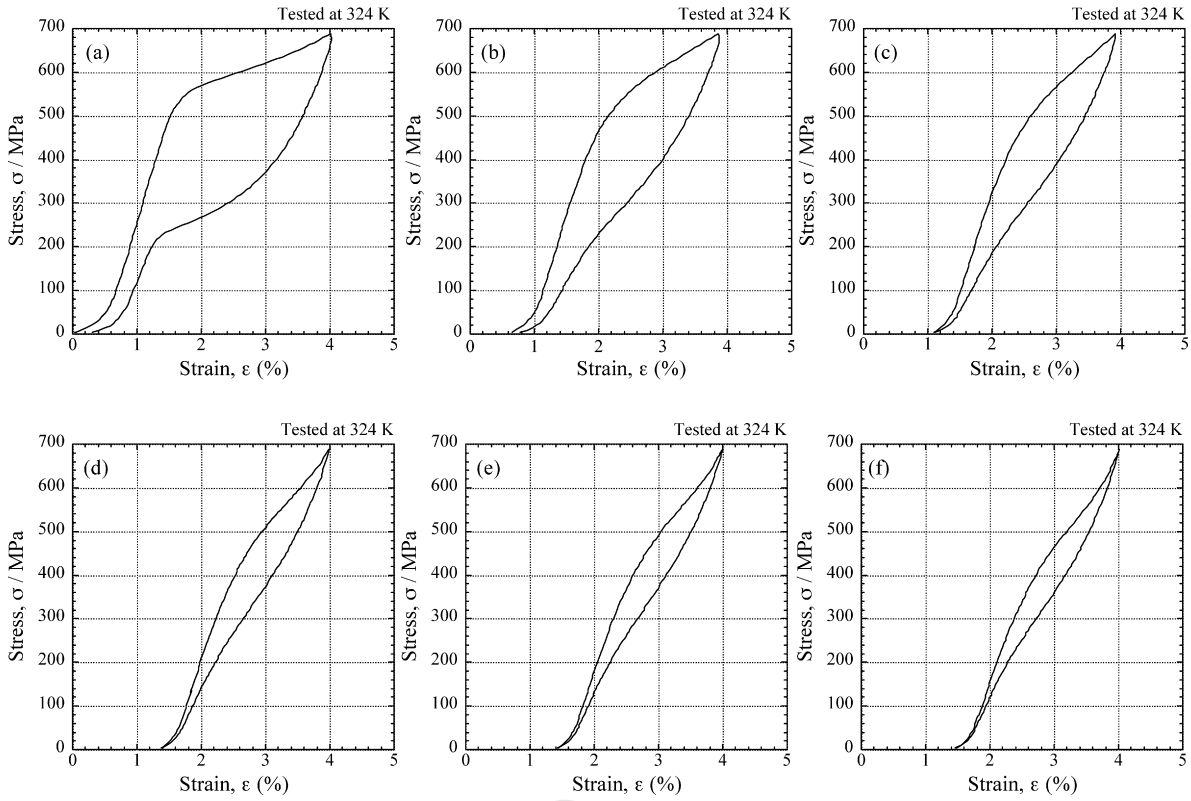

Fig. 10. Changes in stress–strain curves by stress cycles in NiTi sample aged at 773 K for 18 ks under vacuum after (a) 1st, (b) 2nd, (c) 10th, (d) 50th, (e) 100th and (f) 200th cycles.

strain is positive, and that of plastic deformation is negative. Therefore, the part of SME strain is canceled out by plastic deformation of the austenite phase. On the other hand, the NiTi sample which has lower transformation temperatures, so that the points of A_s and A_f can exist in the SME (gray) region and larger SME strain was observed in the first heating (see Fig. 7(a)).

The results of stress cycle testing of the NiTi sample aged at 773 K for 18 ks under vacuum are shown in Fig. 10. At the first cycle, the sample exhibits SE behavior with the onset stress of stress-induced martensite being 540 MPa. The first plateau with less steep slope at the beginning of stress–strain curve with 0–0.4% strain may be due to the stress-induced R-phase transformation, because the testing temperature (324 K) is very close to R_s temperature (see Fig. 3(e)). After the unloading, about 0.3% permanent strain is observed. By increasing number of cycles, the permanent strain is accumulated up to 1.4% by 50 cycles. The hysteresis loop in the stress–strain curves after 50 cycles becomes narrower, and the plateau due to R-phase disappeared and the stress-induced martensite transformation plateau being steeper. The sample after 200 cycles still exhibits 2.6% recoverable strain. Furthermore, no cracking was observed on the sample surface after 200 stress cycles. The onset stress of stress-induced martensite decreases with increasing number of cycle, i.e. about 540 MPa at the first cycle being reduced to about 380 MPa after 200 cycles. The strain of plateau region also decreases with increasing number of cycle. By uni-axial cyclic testing, certain dislocations, which provide favorable stress field for formation of martensite, were introduced in the sample, so as to decrease the onset stress for stress-induced martensite.

4. Conclusion

The thick Ni-rich (NiTi) and Ti-rich TiNi (TiNi) shape memory alloys were successfully fabricated by VPS process. Their phase transformation behavior, SME and SE, and mechanical properties were comparable to those of the bulk specimens reported by the previous researchers. The following is the summary of our findings on NiTi and TiNi samples.

4.1. NiTi sample (Ni-rich composition)

The NiTi sample in as-homogenized state did not exhibit significant martensitic and reverse martensitic transformation behavior as evidenced by the DSC study. The subsequent aging at 773 K for 18 ks under air and vacuum condition led to the excellent martensitic transformation behavior. The aged NiTi sample tested at M_f and A_f showed SME and SE, respectively, where the strain measured in the stress–strain curves were more than 2.4% due to SME and 5.0% due to SE, respectively. The thermal cyclic testing under constant stress was performed. The recoverable strain became smaller with increasing number of cycle. After 15 cycles, the strain–temperature curves were nearly saturated. The stress cyclic testing was also conducted, where the permanent strain was introduced during the testing. The plateau region due to stress-induced martensite and its onset stress decreased with increasing number of cycle. The recoverable strain after 200 cycles was 2.6%, which is useful as an actuator material The TEM observation identified the formation of Ti_3Ni_4 precipi-

tates by the aging, responsible for increasing transformation temperatures.

4.2. TiNi sample (Ti-rich composition)

The TiNi sample in as-homogenized state showed clear transformation behavior as evidenced by the DSC measurements. However, the aging treatment did not affect the transformation temperatures. The TiNi sample in the as-homogenized state exhibited SME behavior (4.0% recoverable strain) at RT. The stress–strain curves were obtained at the A_f, where no SE behavior was observed. The TiNi sample has relatively high A_f temperature, so that the degradation of mechanical properties occurred at and above A_f. At these temperatures, the sample was yielded before the formation of stress-induced martensite. During thermal cycle testing, the permanent strain due to the yielding was introduced during first heating and thereafter. The recoverable strain decreased and the strain due to the yielding increased with increasing number of cycle. Finally, the temperature-strain curves are nearly saturated after 15 cycles. The recoverable strain after 15 cycles was about 2.2%, which is also useful as an actuator material.

Acknowledgements

This work was funded by Navy SBIR contract (N68335-04-C-0191). We are thankful for Dr. K. Kikuchi, University of Washington, for her help in the DSC analysis.

References

[1] H. Nakayama, K. Tsuchiya, Z.G. Liu, M. Umemoto, K. Morii, T. Shimizu, Mater. Trans. 42 (2001) 1987–1993.
[2] K. Otuska, C.M. Wayman (Eds.), Shape Memory Materials, Cambridge University Press, 1998 (chapter 6).
[3] H. Kato, T. Koyari, S. Miura, K. Isonishi, M. Tokizane, Scripta Metall. 24 (1990) 2335–2340.
[4] H. Kato, T. Koyari, M. Tokizane, S. Miura, Acta Met. Mater. 42 (1994) 1351–1358.
[5] M. Bram, A. Ahmad-Khanlou, A. Heckmann, B. Fuchs, H.P. Buchkremer, D. Stöver, Mater. Sci. Eng. A 337 (2002) 254–263.
[6] L. Krone, E. Schüller, M. Bram, O. Hamed, H.P. Buchkremer, D. Stöver, Mater. Sci. Eng. A 338 (2004) 185–190.
[7] B. Bertheville, J.-E. Bidaux, Scripta Mater. 52 (2005) 507–512.
[8] A.P. Jardine, Y. Field, H. Herman, Scripta Metall. 24 (1990) 2391–2396.
[9] A.P. Jardine, Y. Field, H. Herman, J. Mater. Sci. Lett. 10 (1991) 943–945.
[10] H. Hiraga, T. Inoue, S. Kamado, Y. Kojima, A. Matsunawa, H. Shimura, Surf. Coat. Technol. 139 (2001) 93–100.
[11] M. Bram, A. Ahmad-Khanlou, H.P. Buchkremer, D. Stöver, Mater. Lett. 57 (2002) 647–651.
[12] W. Tang, B. Sundman, R. Sandström, C. Qiu, Acta Mater. 47 (1999) 3457–3468.
[13] H. Funakubo (Ed.), Shape Memory Alloys, Gordon and Breach Science Publishers, 1987 (chapter 2).
[14] T. Tadaki, Y. Nakata, K. Shimizu, K. Otsuka, Trans. JIM 27 (1986) 731–740.
[15] F. Lopez, A. Salinas-Rodriguez, J.L. Rodriguez-Galicia, Scripta Mater. 34 (1996) 659–664.
[16] Y. Liu, P.G. McCormick, ISIJ Int. 29 (1989) 417–422.
[17] K. Otuska, C.M. Wayman (Eds.), Shape Memory Materials, Cambridge University Press, 1998 (chapter 1).